Influence of ion-electron interaction on the formation mechanism of depleted zones in displacement cascades in metals

V. G. Kapinos* and D. J. Bacon
Department of Materials Science & Engineering, The University of Liverpool, P.O. Box 147, Liverpool, L69 3BX, United Kingdom
(Received 10 January 1994; revised manuscript received 21 May 1994)

The mechanism of redistribution of vacancies in the depleted zone of a displacement cascade in copper has been investigated by molecular-dynamics simulations. A simplified model of the thermal spike was used, for which the calculation cell was cooled down along one axis after vacancies and kinetic energy had been introduced in the center of it. The influence of electron-phonon coupling on the sweeping of vacancies in this highly disordered hot core as it cools was then investigated. The characteristic cooling time, τ, for transfer of heat to the electron system by ion-electron interaction was a variable parameter and was varied from 1 to 10 ps. According to Finnis *et al.* [Phys. Rev. B **44**, 291 (1991)] the values of $\tau \leq 1$ and $\tau \geq 5$ ps are typical of metals such as Ni and Cu, respectively. In the conditions of the nonuniform distribution of the thermal spike, the maximum size of the real melt becomes a function of τ. The influence of the strong coupling on the vacancy redistribution is more strongly pronounced for thermal spikes in which the average atomic kinetic energy in the melt is close to the value $(3k_B T_m + L)$, where T_m is the melting temperature and L is the latent heat of fusion. In this case the time to form the liquid structure by melting is comparable with the time to cool the zone to below the temperature of crystallization. It has been demonstrated that the coupling also influences the number of vacancies trapped by the melt during the advance of the solid/liquid interface. It is shown that in metals with strong electron-phonon coupling, the highly disordered structure of the melted region can be frozen in when a depleted zone with a high concentration of vacancies ($\geq 2-5$ at. %) solidifies.

I. INTRODUCTION

An earlier paper[1] reported on a molecular-dynamical investigation of the formation mechanism of depleted zones in displacement cascades with a melted core. It was shown that in the nonuniform temperature field of the thermal spike during crystallization of this core, vacancies are swept to the center of the spike as a result of the advance of the solid/liquid interface. This effect leads to the development of a zone where the average concentration of vacancies is several times larger than that produced before the onset of the thermal spike phase. A model for interpretation of the computer simulation results was proposed, based on the assumption, which is consistent with simulation data, that the total pressure in the melted region is constant and does not depend on position. According to this model, the vacancy-sweeping mechanism is a consequence of the formation of compressed liquid layers at the solid/liquid interface under the influence of a large temperature gradient (10^2-10^3 K/nm).

This model is applicable only if the cascade core really is molten. A necessary condition for this is that the average kinetic energy per atom in the hot cascade core is higher than the value $(3k_B T_m + L)$, where k_B is Boltzman's constant, T_m is the melting temperature, and L is the latent heat of melting.[2] Although the core structure of these cascade has been described as liquidlike,[3,4] the period of quenching of low-energy cascades is of the order of a picosecond and is comparable with the time of the full melting phase transition.[5] Furthermore, the formation of real liquid structure may be questionable, even for high-energy cascades, if the lifetime of the spike is short due to strong electron-ion interaction, i.e., if heat can be extracted rapidly from the ionic system by strong coupling between phonons and electrons.[6]

Finnis, Agnew, and Foreman[6] have incorporated a simplified model of the electron-phonon interaction into a molecular-dynamics (MD) code. Their simulations of cascades in Cu in the energy range 250 eV–1 keV did not show noticeable influence of the electron-phonon coupling on the net number of surviving defects, but did indicate that it influences the length of replacement collision sequences in Ni, thus reducing the number and/or concentration of vacancies in the melted zone. However, it is difficult to investigate the influence of electron-phonon coupling on depleted-zone formation in a systematic fashion for high-energy cascades, because of the variability of cascades in three dimensions, the computing resources required for their simulation, and the problems associated with analyzing the cascade parameters in such complex structures. The aim of the present work was to overcome these difficulties by extending the use of our previous one-dimensional model of the thermal spike,[1] but modified to take into account the electron-phonon coupling. The advantage of this approach is that it enables the thermodynamic and defect properties of the spike zone to be assessed as the strength of the coupling is varied, but with other key parameters held constant.

II. THE COMPUTATIONAL MD MODEL

The temperature T_i of the ions in the thermal spike with the electron-phonon interaction included can be calculated using the expression[6]

$$\frac{\partial T_i}{\partial t} = \left[\frac{k_i}{c\rho}\right]\nabla^2 T_i - \frac{T_i - T_e}{\tau} , \quad (1)$$

where k_i is the lattice thermal conductivity, c is the heat capacity per unit volume, ρ is the density, T_e is the local electronic temperature, and τ is the characteristic cooling time for transfer of heat to the electron system by ion-electron interaction, which may be obtained from the expression[6]

$$\tau = \frac{\pi^2 r_0 c\rho T_0}{3\Theta_D \gamma_e T_e v_F} \quad (2)$$

where γ_e is the coefficient of the electronic heat capacity per unit volume, r_0 is the radius of the Wigner-Seitz cell, v_F is the Fermi velocity, and T_0 is the lattice temperature at which the electronic mean free path is reduced to r_0.

For copper the local electronic temperature T_e remains close to ambient temperature T_c because the time scale for heat conduction through the electron system is shorter than the time scale for transfer of energy to the electrons by the electron-phonon mechanism,[6] whereas in Ni the electrons may be heated significantly in the thermal spike because of the strong electron-phonon coupling in this metal. Finnis, Agnew, and Foreman[6] estimated the values of τ in Cu and Ni and showed that they are around 5 and 0.1 ps, respectively, with an electron temperature of 300 K. Increasing T_e above 300 K shifts the estimated τ to slightly lower values especially at the beginning of the cooling of the thermal spike (see the Appendix). A solution of the heat transfer equation (1) under the condition that T_e is a constant, T_c, has the form

$$T_i = \exp\left[-\frac{t}{\tau}\right] T(t,\mathbf{r},k_i) + T_c , \quad (3)$$

where $T(t,\mathbf{r},k_i)$ is the temperature distribution which is independent of τ but depends on the thermal conductivity k_i.

To include the electron-phonon coupling in a molecular-dynamic simulation under these conditions, all ionic velocities, defined by a standard iteration scheme, are scaled at each time step n by an appropriate amount depending on the local ion temperature

$$v_{n+1} = v_n \sqrt{\beta} , \quad (4a)$$

where

$$\beta = \frac{T_{n+1}}{T_n} = \exp\left[-\frac{t_0}{\tau}\right] , \quad (4b)$$

where t_0 is the time step. (A value of t_0 of 4×10^{-15} s was used here.)

Parameter τ is variable in our investigation and was varied from 1 to 10 ps. For values of $\tau > 10$ ps, the influence of the electron-phonon interaction on the lifetime of the melted zone is negligible and the relaxation of the thermal spike energy depends only on the value of the lattice conductivity k_i. The results for $\tau < 1$ ps were found to be qualitatively the same as those for $\tau = 1$ ps.

To investigate the effects of τ on cascade phenomena in a systematic manner, the energy dissipation process was simulated in a rectangular calculation cell extended along the x axis and consisting of 15 000 movable atoms. The crystal structure was fcc and the dimensions of the cell were $150a_0 \times 5a_0 \times 5a_0$, where a_0 is the lattice parameter. The calculation cell had rigid boundary conditions along the [100] x axis and periodic ones along the transverse y and z axes [010] and [001], respectively. The cell volume was divided along the x axis into equal layers with thickness equal to the lattice parameter, i.e., each layer contained two (200) atomic planes of 50 atoms each in the perfect crystal. Each of the layers was labeled by an index $j = 1, 150$.

The same number of atoms was randomly removed from each atomic plane initially so that the vacancy distribution was uniform along the x axis and the average vacancy concentration corresponded to a specified quantity $\langle C_v \rangle$. A one-dimensional thermal spike was then introduced at zero time with a Gaussian temperature profile along the x axis.[2] The maximum initial temperature in the profile was 3876 K (1 eV/atom) and the width was $6a_0$. The initial temperature profile produced the melting transition in the central part of the cell and during the first 400–500 time steps the volume per atom in the central layer increased, irrespective of the value of $\langle C_v \rangle$. The volume expansion produced during the melting transition achieved a value of approximately 18–20 % for $\langle C_v \rangle = 0$ at. %. This level of the expansion was then maintained in the next 1500 time steps but the temperature in this layer decreased during the same time interval. The volume change during melting was 4.5%, representing 25% of the total expansion. The remaining part of the expansion was due to liquid thermal expansion. The phase transition from solid to liquid was completed in the first 100–200 steps (≈ 0.4 ps).

As a consequence of thermal expansion, large fluctuations of pressure and density appeared in the cell. Elastic waves which stress the material up to 0.1 of the bulk modulus B were generated during the expansion of the heated layers and traveled along [100] with the longitudinal sound velocity 6.4×10^5 m/s. The thermal spike generates nonsteady waves, characterized by a continually growing length of nonequilibrium material immediately following the wave fronts. Unless precautions are taken, the waves reflect from the boundaries of the cell and after some time interact with each other in the center part of the cell, thus influencing the thermal spike behavior. To damp this influence we used a special procedure to reduce the quantity of the reflected energy. This procedure was based on the freezing of the positions of the atoms in a few layers adjoining the rigid boundaries of the cell along the x axis. The freezing was started at the moment of time when the pressure in these layers achieved a maximum.

We have used for this work the many-body interatomic potential for Cu derived in Ref. 7, but modified as described in Ref. 8 to reproduce the pressure-volume relationship of pure copper and to provide better treatment of interactions inside the normal nearest-neighbor distance of $a_0/\sqrt{2}$. The equilibrium melting point of copper with this model is 1200–1300 K (see next section).

As a parameter characterizing the kinetics of disordering of the crystal structure in the heated crystallite, the planar structure function[9] is used

$$S_\chi(t)=\sum_{n=1}^{N}\cos\frac{4\pi}{a_\chi}[\chi_n(t)-\chi_n(0)]\ , \tag{5}$$

where a_χ is the distance between atomic planes in the direction of χ ($\chi\equiv xy,z$); $\chi_n(0)$ and $\chi_n(t)$ are the χ coordinates of the nth atom at the initial time and at time t, and N is number of atoms in two atomic layers $75-j$ and $76+j$ ($j=0$–74). For the crystal $S_\chi(t)\approx N$, which is 200 in our case, but for the liquid it oscillates about zero with an amplitude $\approx\sqrt{N}$.

The vacancies are swept to the center of the thermal spike under the effect of the nonuniform temperature distribution. The strength of the sweeping effect is proportional to the parameter G^* [Ref. 1, formula (10)]

$$G^*=\sum_{i=1}^{N_{\rm melt}}\left[\frac{(B\beta^*-\alpha+\alpha\beta^*T^i)T^i}{B+\alpha T^i}-\frac{(B\beta^*-\alpha+\alpha\beta^*T^k)T^k}{B+\alpha T^k}\right], \tag{6}$$

where $N_{\rm melt}$ is the number of melted layers, k is any arbitrarily selected number among the numbers of the melted layers, $\alpha=3\gamma k_B/\Omega_0$, $\beta^*=\xi\alpha/B$, ξ is a parameter, which is defined by the condition of equilibrium between the heated-up region and the surrounding elastic matrix, ($\xi<1$), T^i is the temperature in the ith layer, γ is the Gruneisen parameter, B is the bulk modulus of the liquid, and Ω_0 is the volume per atom in perfect lattice at $T=0$ K. Expression (6) can be rewritten as

$$G^*=\sum_{i=1}^{N}\left[\left[\xi\beta-\frac{\beta}{1+\beta T^i}\right]T^i-\left[\xi\beta-\frac{\beta}{1+\beta T^k}\right]T^k\right]$$
$$\approx(\xi-1)\beta\sum_{i=1}^{N}(T^i-T^k)\ . \tag{7}$$

To analyze the simulation results the parameter

$$G=\frac{G^*}{|\xi-1|\beta} \tag{8}$$

is used. This parameter characterizes the nonuniformity of the temperature distribution in the thermal spike. Large values correspond to the distributions with large thermal gradients.

III. RESULTS

A. Low vacancy concentration ($\langle C_v\rangle=2$ at. %)

The changes with time of the temperature in the central layers 75 and 76 ($j=0$) for different τ are presented in Fig. 1. All curves demonstrate a spike of the temperature near the crystallizing point. For $t=10$ ps the crystallization starts in the central layers at $2800t_0$, when the temperature falls to 1200–1300 K, and is completed after 3000–$3200t_0$. For $\tau=5$ ps the crystallization occurs at approximately the same temperature, but is completed after $2200t_0$. For $\tau=1$ ps the central layer is supercooled and crystallization occurs in the temperature range 800–1000 K.

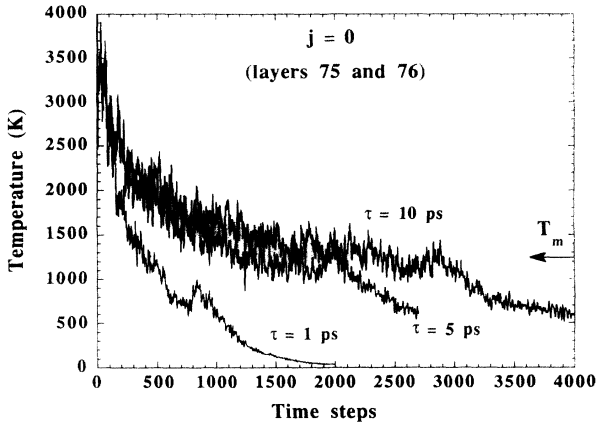

FIG. 1. Variation of the temperature with time in the central layers of the calculation cell for τ values in the range 1–10 ps as indicated. These layers have index $j=0$ (see text). The equilibrium melting point, T_m, is indicated. The vacancy concentration in the calculation cell was 2 at. %.

The kinetics of the melting and crystallization of the different layers can be analyzed using the structural function $S_\chi(t)$. The time dependence of $S_y(t)$ for the layers with $j=0$, 2, 3, and 4 in a calculation cell with $\langle C_v\rangle=2$ at. % for $\tau=1$ and 10 ps is shown in Fig. 2. It is clear that the nonuniform high-temperature distribution leads to melting of the central layers with $j=0$–4 and movement of the liquid/solid interface towards the center of the calculation cell. The time, t_m, when the liquid structure of the layers becomes established is defined as the moment when the S_y curve first crosses the t axis at $S_y=0$. It is approximately $10t_0$ for the layers with $j\le 2$ [Figs. 2(a) and 2(b)] and does not depend on the choice of τ. For $j=3$ [Fig. 2(c) and 4 (Fig. 2(d)] the values of t_m are $200t_0$ and $400t_0$, respectively for $\tau=10$ ps but could not be defined for $\tau=1$ ps because the time of cooling of these layers was comparable with the time required for their disordering.

The time to melt a layer is a function of the initial overheating and depends on the initial layer temperature in accordance with the plot in Fig. 3, which was obtained for various τ and peak temperature values. For an initial kinetic energy per atom more than 0.9 eV/atom (3500 K) the influence of τ on t_m in copper is negligible but near the temperature $T=T_m+L/3k_B=1900$ K, where T_m is the melting temperature and L is the latent heat of melting, it is readily anticipated that this influence is strong on account of the large value of t_m. For instance, the initial temperature of the layers with $j=4$ is approximately 2500 K and the time for melting them is 300–$400t_0$, i.e., about 1.6 ps, for $\tau=10$ ps. However, the temperature of these layers after the first 100 steps for $\tau=1$ ps decreased in such a way that the ordering of the atomic positions started before the melted state had been achieved [Fig. 2(d)]. This means that the maximum size of the melted region in the crystal with strong electron-phonon cou-

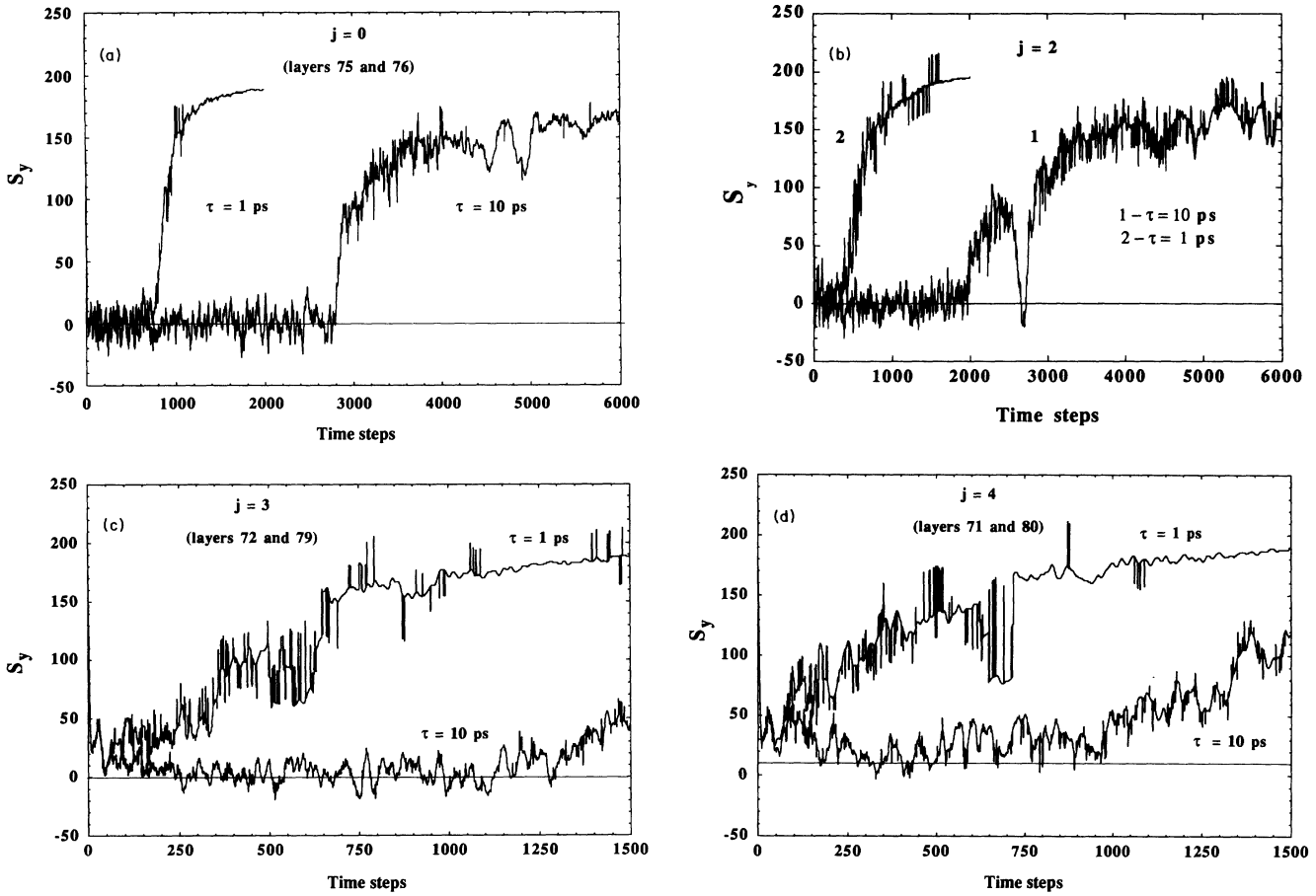

FIG. 2. The planar structure function, S_y, as a function of time and τ for different layers as indicated. The vacancy concentration in the calculation cell was 2 at. %.

pling (τ less than 1 ps) becomes a function of not only the initial kinetic-energy distribution but also the coupling, because the boundary of the melt is defined not only by the initial overheating above the melting point but also by the total time available for the solid-liquid transformation. This time interval can be estimated from Fig. 3.

Now we consider the vacancy distributions in the layers near the center of the calculation cell after crystallization. The final distribution of the vacancies for $\langle C_v \rangle = 2$ at. % immediately after crystallization for the three values of τ equal to 10, 5, and 1 ps is shown in Fig. 4, where the number of vacancies, N_v, in each atomic plane of 50 lattice sites is plotted against layer number. The maximum size of the melted region for each τ defined according to the behavior of $S_y(t)$ is marked in the figures. It can be seen that as a result of movement of

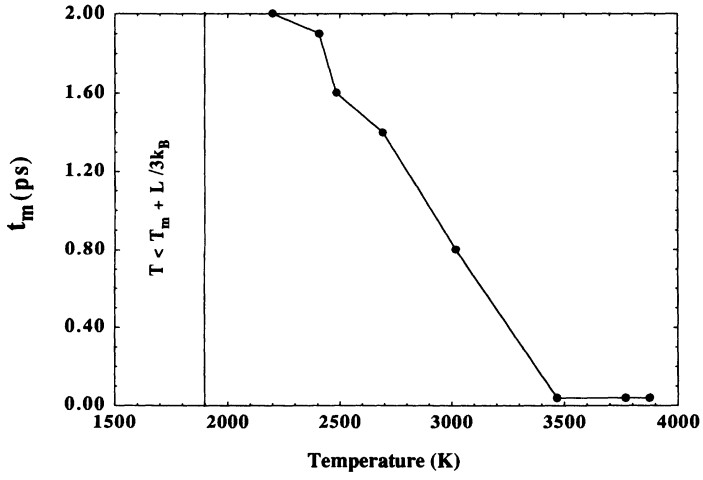

FIG. 3. The change with the initial temperature of the time t_m to achieve the liquid state ($S_y = 0$). The temperature region in which melting cannot be achieved is indicated.

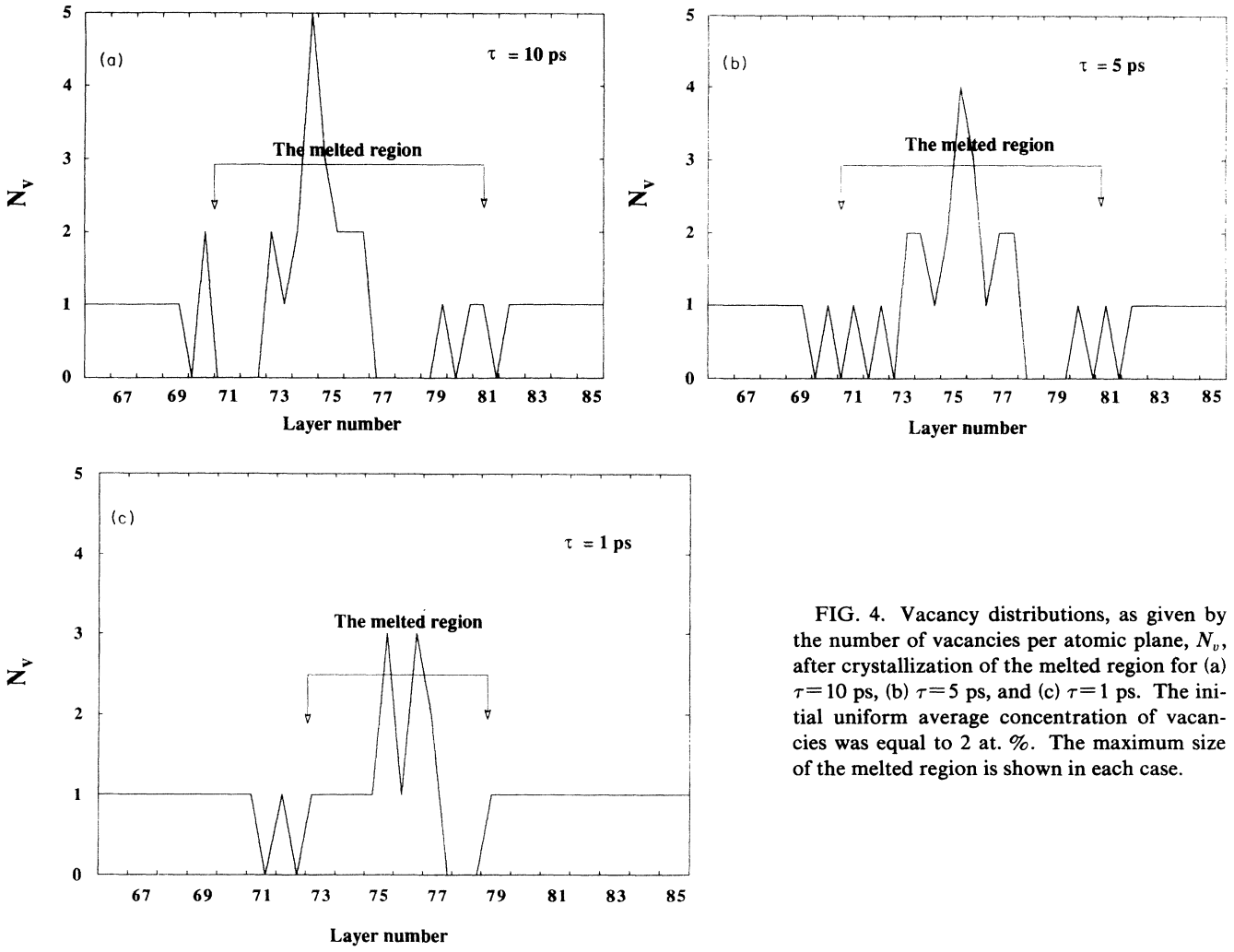

FIG. 4. Vacancy distributions, as given by the number of vacancies per atomic plane, N_v, after crystallization of the melted region for (a) $\tau=10$ ps, (b) $\tau=5$ ps, and (c) $\tau=1$ ps. The initial uniform average concentration of vacancies was equal to 2 at. %. The maximum size of the melted region is shown in each case.

the liquid/solid interphase boundaries most of the vacancies are collected in a few central layers. The concentrations at the maximum of this distribution are 10, 8, and 6 at. % for $\tau=10$, 5, and 1 ps, respectively. After boundary movement the average vacancy concentrating in the peripheral layers of the melted region is decreased to ≤ 0.2 at. % for $\tau=10$ ps and approximately to 0.5 at. % for $\tau=5$ ps. For $\tau=1$ ps the vacancy-sweeping mechanism is less pronounced.

The parameter $G(t)$ [Eqs. (7) and (8)] within the melt defined as above was calculated and is presented in Fig. 5 for $\tau=5$ and 10 ps. It is seen that $G(t)$ is independent of τ only in the first 250 steps. After this time the influence of the temperature gradients on the crystallization of the melt becomes a function of τ. The behavior of $G(t)$ can be explained by the overcooling of the liquid and depression of the solidification temperature of the peripheral layers of the melt for small values of τ. The reduction of $G(t)$ during the solidification of the melt is one of the causes of the reduction of the vacancy sweeping effect for $\tau=1$ ps [Fig. 4(c)].

Vacancy diffusional jumps outside the melt near the liquid/solid boundary are an additional mechanism for the influence of τ on the final vacancy redistribution. It is seen from Figs. 4(a) and 4(b) that the uniform distribution of the vacancies is changed not only in the melted region but also in the crystalline matrix nearby. This indicates that the vacancies have performed diffusional jumps from the solid into the melt. As the liquid/solid interface advances in the first stage of resolidification, some of these vacancies are retained in the new crystal, but we observed from computer graphics that some were able to jump again into the melt. These diffusional jumps of vacancies outside the melted region increase the number of vacancies in the melt and thus raise the final average concentration of the vacancies in the central layers.

B. High vacancy concentration ($\langle C_v \rangle \geq 4$ at. %)

The process of the vacancy redistribution in the calculation cell is changed when the value of $\langle C_v \rangle$ is increased. For $\tau \geq 5$ ps the vacancy distributions are similar to those in Figs. 4(b) and 4(c) and are considered below. The principal differences in the distributions appear when τ is reduced to values less than 3 ps. In these cases the crystal structure of the central layers ($j=0,1$) is not formed after cooling and an amorphous structure is maintained even when the temperature of the layers is re-

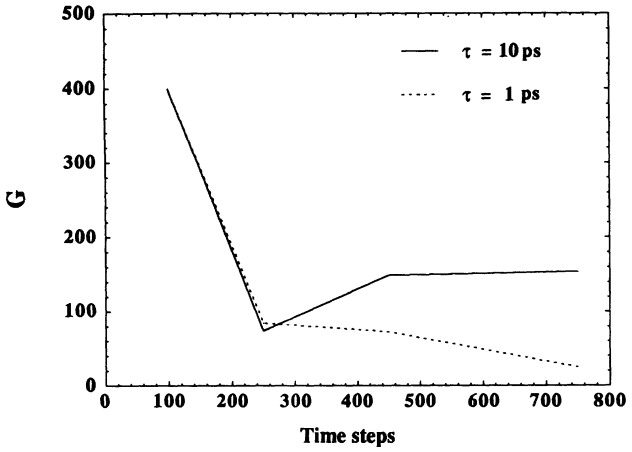

FIG. 5. Parameter G [Eqs. (7) and (8)] for the melted region as a function of time for the two values of τ as indicated. This parameter reflects the nonuniformity of the temperature distribution within the melted region and characterizes the "sweeping" effect.

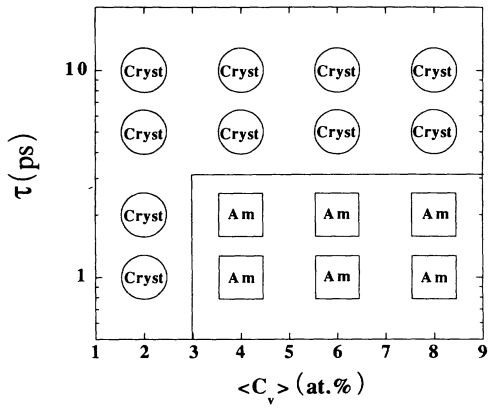

FIG. 6. Diagram showing the resulting structure after solidification for various values of τ and $\langle C_v \rangle$. The circles show the range of the parameters when the crystal structure is recovered, and the squares show the range when a minimum of one layer with amorphous structure was identified after cooling down to 500 K.

duced to 500 K or less. The influence of τ on the recovery of the melted region is shown schematically in Fig. 6. The circles show the range of τ and $\langle C_v \rangle$ for which the crystal structure is recovered after complete cooling of the calculation cell, and the squares show the range when a minimum of one amorphous layer was found after cooling.

The vacancy distributions for $\langle C_v \rangle = 4$ at. % are shown in Fig. 7 for $\tau = 10$ and 5 ps. An extremely high level of $\langle C_v \rangle$ (28 at. % in the peak) was registered for the vacancy distribution with $\tau = 5$ ps. For $\tau = 10$ ps a very interesting effect occurred on crystallization, when one central atomic plane disappeared and two with interstitials were created. One plane consisted of four and the other of five interstitials, which together formed one interstitial dumbbell and an interstitial loop in the (011) plane of eight interstitials. The reason why the different structures formed is that the number of vacancies trapped in the melted region during the liquid-solid interface movement is more for $\tau = 10$ ps than for $\tau = 5$ ps. For one atomic plane to completely disappear it would have been necessary for 50 vacancies to collect together in it. For $\tau = 10$ ps, however, only 41 vacancies were swept and the missing vacancies in the central layer were generated by the production of the excess of nine interstitial atoms in the adjacent atomic planes. The sweeping effect for $\tau = 5$ ps collected only 24 vacancies in two central layers, which was not enough to give the complete collapse effect because the generation of the 26 interstitials required was energetically unfavorable. These vacancies therefore formed only the depleted zone with a high concentration of vacancies seen in Fig. 7.

The vacancy distributions for $\langle C_v \rangle = 8$ at. % are shown in Fig. 8, where the maximum size of the melted zone is shown also. These distributions are very similar to each other. Outside the melt a smooth concentration gradient occurs. The same behavior in the vacancy distribution has been pointed out by Swygenhoven and Caro,[2] and can be explained by the high vacancy mobility in the solid with a high level of vacancy concentration.[10] The count of the vacancies shows that two atomic planes, which are not printed in the figure, disappeared for both $\tau = 5$ and 10 ps. The similarity of the final distributions is the result of the high mobility of the vacancies crystallized outside of the melt. The density of the melt for $\langle C_v \rangle = 8$ at. % is so low that the vacancies, which are crystallized in the solid behind the advancing liquid/solid interface, have an anisotropic migration barrier which permits them to jump back into the melt with high probability. As a result of this, approximately the same quantity of vacancies takes part in the collapse process after crystallization of the melt for both τ values. Unfortunately we could not estimate separately the effect on the total number of vacancies in the melt of the anisotropic diffusion of vacancies in the solid near the solid/liquid interface. It has to be stressed that all registered jumps of the vacancies were towards the melt and can be explained only with the existence of a strong anisotropy in the vacancy diffusion.

C. Some specific features of the crystallization process

The temperature curves in Fig. 1 show a peak just before crystallization. The heights of the peaks are nearly the same and equal to 200–300 K. The peaks appear at the time when the $S_y(t)$ curves dip sharply for the layers with $j \geq 1$ [see, for example, Fig. 2(b)]. Analysis of the atomic structure of the calculation cell before and after the dip shows that the atomic planes are bent by shearing along the [010] direction (but not [001]) for a short time interval. The deformation of the atomic planes at the time $2700t_0$ in the calculation cell with $\langle C_v \rangle = 2$ at. % is shown in Fig. 9. To demonstrate the bending more clearly the scale has been stretched in the [010] direction. The physical reason for the observed temperature and structure behavior is the realization of the latent heat in

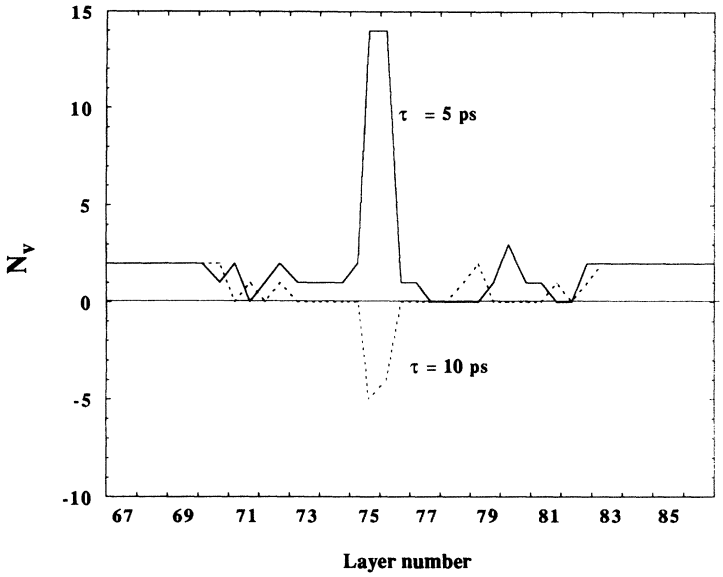

FIG. 7. Vacancy distributions in the calculation cell after crystallization of the melted region for $\tau=5$ and 10 ps. The initial uniform average concentration of vacancies was 4 at. %. For $\tau=10$ ps two atomic planes with nine interstitials were formed. These planes are shown by a negative number of vacancies.

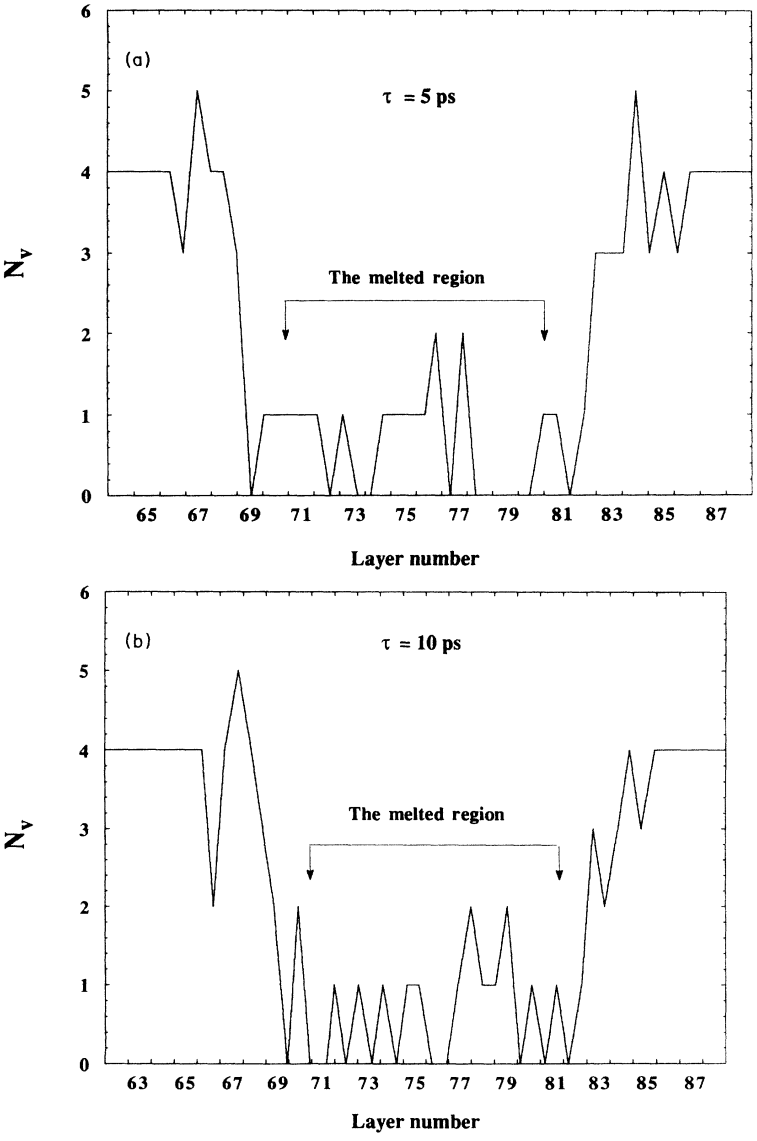

FIG. 8. Vacancy distributions in the calculation cell after crystallization of the melted region for (a) $\tau=5$ ps and (b) $\tau=10$ ps. The initial uniform average concentration of vacancies was equal to 8 at. %. Two atomic planes consisting 50 atoms each have disappeared after "collapse" of the depleted zone.

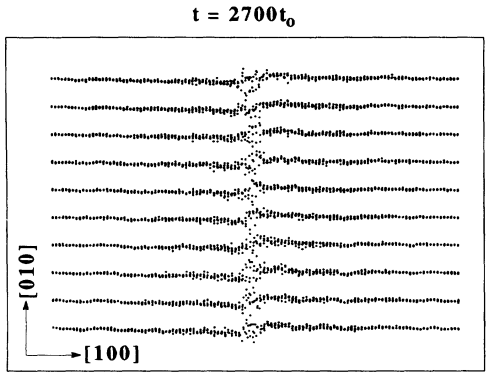

FIG. 9. [001] projection of positions of atoms of the central part of the calculation cell with 2 at. % vacancies before crystallization. The scale has been magnified along [010]. The [010] projection of the same part of the crystal (not shown) does not exhibit any shear along the [100] direction.

short-time interval during which the supercooled liquid is transformed into the solid state. The surrounding matrix is deformed and compressed by the increase in the temperature of the central layers during the liquid-solid transformation. The easiest way to accommodate the atomic plane deformation associated with this in our cell geometry is by shear in either the [010] or [001] directions. Our calculations show that the system selects one of these ways randomly.

The spikes on the temperature curves were not observed for $\langle C_v \rangle \geq 4$ at. %, possibly because the latent heat decreases with decreasing liquid density.

IV. DISCUSSION

The influence of electron-phonon coupling has been investigated in the approximation that the electron temperature T_e remains constant close to the ambient temperature. In this case the molecular-dynamics simulation method may be used to calculate the temperature distribution in the thermal spike by scaling all velocities after each time step with the value $\exp(-t_0/\tau)$, where t_0 is the time step. With a constant electron temperature of 300 K,[6] the values of τ for Cu and Ni are 4.3 ps and 0.12 ps, respectively. Strong electron-phonon coupling (small τ) causes an increase in the local electron temperature that can lead to a decrease in the value of τ (see the Appendix). In our calculations the constant values of τ were selected in the range 1–10 ps and the lattice conductivity was simulated with an N-body potential for Cu. However, we do not claim to connect the values of τ precisely with any real metal, for the prime purpose of these calculations was to demonstrate the influence of strong electron-phonon coupling on the redistribution of vacancies in depleted zones in thermal spikes. The way to incorporate this coupling in the MD code was the use of viscous forces which act in a simple fashion on the moving atoms. We have found from data not presented here that increasing τ to more than 10 ps does not influence the final distribution of the vacancies, and decreasing it below 1 ps does not influence the qualitative behavior of the system as summarized in Fig. 6.

The vacancies in the melt are swept towards the center of the thermal spike in a nonuniform temperature field as a result of the advance of the solid-liquid interface,[1] and the electron-phonon coupling may influence this sweeping effect. For τ around 1 ps the liquid is crystallized at a temperature which is lower than the thermodynamic melting temperature. In this case, the average temperature gradient in the melt at a time t is decreased because the temperature is scaled by the factor $\exp(-t/\tau)$. The sweeping effect is dependent on the parameter G [Eq. (7)], which is defined by the temperature gradient.

The time of the solid-liquid transformation, t_m, depends on the initial kinetic energy of the atoms in the different layers of the thermal spike E_k. The melting starts when $E_k > E_m = (3k_B T_m + L)$, where T_m is the melting temperature and L is the latent heat. The time of the transformation t_m is smaller the higher the overheating $\Delta E_k = E_k - E_m$. When the value of t_m becomes comparable with the cooling time for the electron-phonon mechanism, the overheated region starts ordering from a state which is closer to the solid than the melt. This means that the peripheral layers of the thermal spike region which potentially receive enough energy to melt ($\Delta E_k \geq 0$) do not have sufficient time to transform into liquid for metals with low values of τ. Our calculations show also that the size of the melted region in metals is decreased if the energy density and the values of τ are low enough. This leads to one possible mechanism for the influence of the electron-phonon interaction on vacancy-defect nucleation in cascades. The bigger the size of the melted region the higher the probability of vacancies being trapped by the melt and the higher the number of swept vacancies.

The simulations of one-dimensional heat flow carried out here show that the melted region in the thermal spike with a high initial average concentration of vacancies ($\langle C_v \rangle \geq 4$ at. %) can crystallize on cooling only if the electron-phonon coupling is not very strong ($\tau \geq 5$ ps). If the values of τ are small enough ($\tau < 5$ ps) an amorphous structure can be frozen in after thermal spike cooling. Such high values of $\langle C_v \rangle$ can be achieved in principle in low-temperature heavy-ion irradiation. Although the creation of truly amorphous zones may be more difficult when three-dimensional heat flow occurs, it is interesting to observe that the formation of an additional population of loops on warming samples of Ni irradiated at 30 K to room temperature suggests[11] that uncollapsed vacancy-rich zones can exist, and that these develop into visible vacancy loops as the temperature of the matrix is increased. No view has emerged as to what the structure of these vacancy-rich zones actually is, but it is quite possible, in the light of the present results, that they have amorphous structure (or at least a spongelike crystal structure) because Ni has a very strong electron-phonon coupling ($\tau \approx 0.1$ ps,[6,14]).

The vacancy clusters nucleated in depleted cascade zones have irregular shapes.[12] If the loop first nucleated in cascade collapse is faulted, it may be stimulated to unfault by other vacancies of the same depleted zone which

are not incorporated into the loop.[13] The origin of this influence is the local strain generated near the loop by the surrounding groups of vacancies, which may provide the essential component of the atomic displacement in the required direction along the habit plane. We have observed another mechanism in the present study of copper for τ in the range 1–10 ps that may influence this displacement during the crystallization stage of the thermal spike (Sec. III C). It is based on the rapid release of local latent heat (see Fig. 1) with a significant increase in pressure ≈ 10 GPa for the depleted zones with average concentration of vacancies ≤ 2 at. %. The volume expansion in the crystallization process is sufficient to deform the surrounding matrix to such an extent that a large component of shear deformation is generated along the habit plane where the vacancy loop has been nucleated. In the constrained geometry of our simulation, it occurred along [010] on the (100) plane, but in an unconstrained, three-dimensional situation, it may arise to unfault Frank loops in the fcc metals by a $\langle 11\bar{2} \rangle \{111\}$ shear.

The depleted zones with an extremely high concentration of vacancies are structurally unstable and collapse into vacancy loops. The one-dimensional model of the thermal spike used here demonstrated an unexpected effect of this collapse, namely when one atomic plane totally disappeared by vacancy aggregation, a small interstitial cluster was created in the adjacent crystallized region to compensate for the additional vacancies required. In our case for $\langle C_v \rangle = 4$ at. % the disappearance of the plane was physically similar to the collapse of an infinite vacancy loop with habit plane (100) and Burgers vector 1/2[100]. This infinite loop had no strain energy, and the energy released during the collapse of one atomic plane was much higher than the additional formation energy of the small interstitial cluster. However, it is not clear that this mechanism could lead to interstitial cluster formation in real cascades, where the cluster would be created in the highly attractive strain field of the finite-sized vacancy loop.

V. CONCLUSIONS

The influence of electron-phonon coupling on the sweeping of vacancies in cascade cores has been investigated using the one-dimensional thermal spike model. A many-body potential for copper was selected to simulate motion of the ion cores by molecular dynamics (MD). To include the electron-phonon coupling in MD, all ionic velocities were scaled at each time step by an amount depending on the parameter τ,[6] which was varied from 1 to 10 ps. The main conclusions are as follows.

(1) In the metals with strong electron-phonon interaction ($\tau \leq 3$ ps) the liquid structure of the melted region is limited by the extremely fast cooling in the depleted zone with a high concentration of vacancies.

(2) The time of the solid-to-liquid transformation depends on the value of the initial kinetic energy in an atomic layer. For energy close to the value $E_k = (3k_B T_m + L)$, where T_m is the melting temperature and L is the latent heat, the time for melting becomes comparable with the time of cooling to the temperature of crystallization if the electron-phonon coupling is strong enough (τ small). In the conditions of the nonuniform temperature distribution of the thermal spike, the maximum size of the real melt is a function of the value of τ.

(3) The average concentration of vacancies in the depleted zone after crystallization depends on the value of τ. Strong coupling reduces the number of vacancies and the average vacancy concentration in the depleted zone. This is explained by the reduction of the average temperature gradients and, hence, the strength of the sweeping effect. The coupling also influences the velocity of advance of the solid/liquid interface. Vacancies formed in the solid behind the interface can make diffusional jumps back into the liquid, but this effect is much reduced by strong coupling.

ACKNOWLEDGMENTS

The authors wish to thank the EPSRC for financial support and Dr. A. F. Calder for assistance with the organization of the computations carried out at Liverpool.

APPENDIX: THE ELECTRON TEMPERATURE IN A CASCADE

The electron mean free path in the temperature field of the thermal spike in the harmonic approximation is estimated by expression[14]

$$\lambda = r_0 T_0 / T_i \quad (T > \Theta_D) , \tag{A1}$$

where r_0 is the radius of the Wigner-Seitz cell, T_0 is the value of the lattice temperature at which λ is reduced to r_0, Θ_D is the Debye temperature, and T_i is the ion temperature. The ion temperature in the thermal spike is not uniform and the average value of T_i has to be used: $T_i = \langle T_i \rangle$.

To estimate $\langle T_i \rangle$ corresponding to a thermal spike associated with a displacement cascade created by a primary knock-on atom of damage energy E_{dam}, a thermal spike model with the initial Gaussian distribution of temperature may be used:

$$T(r,0) = \frac{\Omega E_{\text{dam}}}{3k_B (\pi R_{\text{th}}^2)^{3/2}} \exp(-r^2/R_{\text{th}}^2) + T_c , \tag{A2}$$

where R_{th} is the characteristic size of the thermal spike, T_c is the ambient temperature, and Ω is the volume per atom. $\langle T_i \rangle$ is then given by

$$\langle T_i \rangle = \frac{3}{R^3} \int_0^R r^2 T(r,t) dr , \tag{A3}$$

where R is the radius of the spherical central region of the thermal spike. The diffusional approach is used to calculate the spatial temperature distribution of the electrons within this region. This approach is valid only when the mean free path of an electron $\lambda = r_0 T_0 / \langle T_i \rangle$ satisfies the condition: $\lambda \ll R$.

Atoms of moderate atomic weight, such as Cu and Ni, have thermal spikes with maximum energy of 20–30 keV

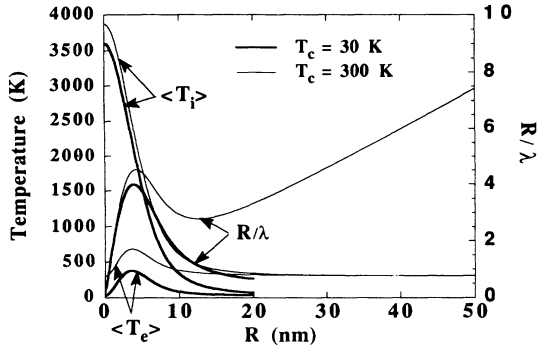

FIG. 10. Variation of the mean temperatures $\langle T_i \rangle$ and $\langle T_e \rangle$ for the ions and electrons, respectively, inside spheres of radius R for a spherical 30 keV cascade at time $t=10^{-13}$ s. The ambient lattice temperature T_c is taken to be equal to either 30 or 300 K. The ratio of the cascade radius R to the electron mean free path λ is also shown.

due to subcascade formation at higher energy. Values of $E_{\rm dam}=30$ keV, $R_{\rm th}=4.0$ nm and $T_c=30$ and 300 K were used in the calculations presented below.

The curves plotted in Fig. 10 demonstrate the behavior of $\langle T_i \rangle$ and the ratio R/λ as functions of R at $t=10^{-13}$ s. The bold and thin lines on the figure are for $T_c=30$ and 300 K, respectively. It is seen that a maximum value of R/λ of about 4 is achieved at $R=4-5$ nm for both T_c values when the average temperature of the central part of the spike is 2200–2300 K. For $T_c=300$ K a value of R/λ more than 4 can also be achieved for $R>30$ nm, but at this distance $\langle T_i \rangle$ falls very close to the ambient temperature. To estimate the spatial temperature distribution of the electrons we assumed that it is reasonable to use the diffusion approximation within the region with $R<5-6$ nm. Diffusion in the electronic system is much faster than in the ionic one, so a steady-state equation for the temperature distribution of the electrons, $T_e(r,t)$, can be used:[6]

$$\frac{\nu_F r_0 T_0}{3\langle T_i \rangle}\nabla^2 T_e + \left[\frac{3\Theta_D \nu_F}{\pi^2 r_0 T_0}\right](\langle T_i \rangle - T_e)=0 , \qquad \text{(A4)}$$

where ν_F is the Fermi velocity. The initial electron temperature distribution is equal to the ambient temperature: $T_e(r,0)=T_c$ and the boundary conditions are

$$T_e(R,t)=T_c \quad \text{and} \quad \left.\frac{\partial T_e}{\partial r}\right|_{(0,t)}=0 , \qquad \text{(A5)}$$

where R is the radius of the central part of the thermal spike, which has an average ion temperature $\langle T_i \rangle$ and in which the diffusional approximation is applicable for electrons. We assume that the ion temperature is equal to the ambient temperature T_c at $r>R$. This assumption reasonably describes the electron behavior outside the hottest part of the thermal spike because the mean free path of the electrons in the region $R<r<R_1$ with average ion temperature

$$\langle T_i \rangle_2 = \frac{3}{R_1^3 - R^3}\int_R^{R_1} r^2 T(r,t)\,dr \qquad \text{(A6)}$$

gives a mean free path $\lambda_2 = r_0 T_0 / \langle T_i \rangle_2$ which is considerably less than the interval $(R_1 - R)$ only for large R_1, when $\langle T_i \rangle_2$ decreases and becomes close to T_c.

For the same values of the parameters which have been used for Ni by Finnis, Agnew, and Foreman[6] we have calculated the distribution of $T_e(r,t)$ as a function of R for $t=10^{-13}$ s, and the average values of the electron temperature $\langle T_e \rangle$ as a function of R for $T_c=30$ and 300 are also presented on Fig. 10. It is seen that the average electron temperature in a spherical cascade in Ni may be twice the ambient temperature when the latter is 300 K. This means that at the beginning of the thermal spike the electron-phonon coupling parameter estimated in expression (2) of the present paper has to be two times stronger on average than it would if defined by $T_e=T_c=300$ K. But for $T_c=30$ K the electron temperature can be ten times higher than that of the lattice. We conclude that the assumption $\langle T_e \rangle \approx T_c$ can in principle give a realistic estimate of the electron-phonon coupling for sufficiently high ambient temperature, in our case for $T_c \geq 300$ K.

*On leave from Department of Radiation Materials Science, Russian Scientific Centre "Kurchatov Institute," Moscow, Russia.

[1]V. G. Kapinos and D. J. Bacon, Philos. Mag. A **68**, 1165 (1993).
[2]H. Van Swygenhoven and A. Caro, Phys. Rev. Lett. **70**, 2098 (1993).
[3]T. Diaz de la Rubia, R. S. Averbach, H. Hsieh, and R. Benedek, J. Mater. Res. **4**, 579 (1989).
[4]A. J. E. Foreman, W. J. Phythian, and C. A. English, Philos. Mag. A **66**, 671 (1992).
[5]V. G. Kapinos and P. A. Platonov, Phys. Status Solidi A **90**, 291 (1985).
[6]M. W. Finnis, P. Agnew, and A. J. E. Foreman, Phys. Rev. B **44**, 567 (1991).
[7]G. J. Ackland and V. Vitek, Phys. Rev. B **41**, 10 324 (1990).
[8]H. F. Deng and D. J. Bacon, Phys. Rev. B **48**, 10 022 (1993).
[9]L. Verlet, Phys. Rev. **159**, 98 (1967).
[10]V. G. Kapinos, Yu. N. Osetskii, and P. A. Platonov, J. Nucl. Mater. **184**, 221 (1991).
[11]I. M. Robertson, J. S. Vetrano, M. A. Kirk, and M. L. Jenkins, Philos. Mag. A **63**, 299 (1991).
[12]T. Diaz de la Rubia and M. W. Guinan, Mater. Sci. Forum, **97-99**, 22 (1992).
[13]V. G. Kapinos, Yu. N. Osetskii, and P. A. Platonov, J. Nucl. Mater. **173**, 229 (1990).
[14]C. P. Flynn and R. S. Averback, Phys. Rev. B **38**, 7118 (1988).